A Simplified Equivalent Circuit Model of Series Resonant Converter

Shuilin Tian, *Student Member, IEEE*, Fred C. Lee, *Life Fellow, IEEE*, and Qiang Li, *Member, IEEE*

***Abstract*—Equivalent circuit models are useful design tools for control and have already well served their purposes in pulse width modulation dc–dc converters. However, no simple equivalent circuit model is available yet for resonant-type dc–dc converters. Up to now, the most successful equivalent circuit model of series resonant converter (SRC) is based on extended describing function concept, which was proposed by Yang *et al.* [30]. However, the equivalent circuit is a complicated fifth order with the cross-coupling effect and no analytical solution is provided for transfer functions. This paper proposes a simple third-order equivalent circuit model of SRC. The equivalent circuit model is derived by simplification of the original fifth-order equivalent circuit, based on the fact that the resonant capacitor behaves like an equivalent resonant inductor with respect to the modulation frequency. The equivalent circuit model can predict the dynamic behavior very well when the switching frequency is below, close to, or above the resonant frequency. Furthermore, for the first time, analytical expressions of all transfer functions, i.e., control-to-output, input-to-output, output impedance, and input impedance are provided. These analytical transfer functions will serve as a useful tool for the feedback design. The equivalent circuit model is verified by Simplis simulation and experimental results.**

***Index Terms*—Equivalent circuit model, series resonant converter (SRC), small-signal model, transfer functions.**

I. Introduction

GENERALLY speaking, dc–dc converters can be divided into two categories: pulse width modulation (PWM) converters and resonant converters. As most of the applications involve a regulated voltage output, a feedback loop is incorporated into the control system to stabilize the output voltage. For the optimal design purpose, small-signal models are indispensable. For PWM converters, small-signal models are available to engineers for most of the control methods. 1) For single-loop (voltage mode) control, averaging concept is widely used. This concept was first proposed by Wester and Middlebrook [1] and then represented in the state-space approach by Middlebrook and Cuk [2]. To provide more insights on the circuit level, a three-terminal switch model was proposed by Tymerski *et al.* [3] and Verperian [4]. 2) For current mode control, the inductor current has sideband effect and it causes subharmonic problem in some cases ($D > 0.5$ for the peak current mode) [5].

Manuscript received May 20, 2015; revised June 30, 2015; accepted July 31, 2015. Date of publication August 4, 2015; date of current version December 10, 2015. Recommended for publication by Associate Editor S.-C. Tan.

The authors are with the Center for Power Electronics Systems, The Bradley Department of Electrical and Computer Engineering,Virginia Tech, Blacksburg, VA 24061 USA (e-mail: tianshuilinpe@gmail.com; fclee@vt.edu; lqvt@vt.edu).

Color versions of one or more of the figures in this paper are available online at http://ieeexplore.ieee.org.

Digital Object Identifier 10.1109/TPEL.2015.2464351

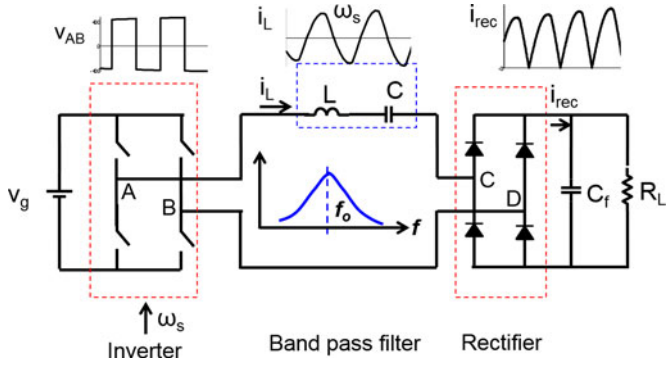

Fig. 1. Diagram of SRC with waveforms of major signals.

In this case, average concept breaks down as the switching frequency components are neglected. A more advanced modeling methodology, the describing function method is successfully applied to all kinds of current mode controls by Li and Lee [5] and analytical transfer functions are derived. To provide more physical insights, unified three-terminal switch models were developed by Yan *et al.* [6] and Tian *et al.* [7]. 3) For V^2 control or ripple-based control methods, both the capacitor voltage and the inductor current have the sideband effects [11]. Analytical small-signal models were derived based on describing function method by Li and Lee [8] and further analyzed by Tian *et al.* [9], [10]. To provide more physical insights, a unified equivalent circuit model for V^2 control was developed in [11]. Therefore, for PWM converters, the feedback design is straightforward with the help of all these research efforts.

However, the scenario is different for resonant converters. The series resonant converter (SRC) is the simplest resonant converter. The schematic of the full-bridge SRC is shown in Fig. 1. It has been used widely for power conditioning in the sophisticated aerospace industry [12]–[16] and in some industrial applications such as laser power supply applications [17]. The state-space averaging method breaks down for resonant converters. The reason is that for resonant converters, some of the state variables do not have dc components but contain strong switching frequency component and its harmonics, whereas the dc components are the dominant parts of the state variables for PWM converters. Due to the strong oscillatory nature of resonant states, the switching frequency interacts with the natural resonant frequency. This results in an interesting phenomenon which is often referred to as the beat frequency dynamics where the high-frequency response is determined by a pair of double pole located at the beat frequency [26]. This interaction cannot be investigated using the averaging concept because it eliminates the switching frequency information.

Several methods are presented to successfully capture beat-frequency dynamics: the first method was proposed by Vorperian and Cuk from combination of state-space analysis without linear ripple approximation in time-domain and discrete-time analysis [18]. The modeling results of control-to-output voltage and input to output voltage transfer functions are shown to be very accurate experimentally with the capability of capturing beat-frequency dynamics. However, the results obtained are computed numerically because of the occurrence of functions of matrices which are difficult to determine in expression form. The second is the sampled-data method or discrete-time analysis [19]–[22]. The discrete model captures the inherent sampling nature and can predict the small-signal behavior up to the switching frequency. However, the sampled-data analysis and discrete analysis technique is very difficult to extract physical insight and is too complex for practical use. The third method is the generalized averaging concept [23], [24]. An effort was made by Sander *et al.* [23] to extend the state-space averaging technique to model the resonant converters. The derived model can correctly predict the beat frequency dynamic, however, it only proposes the modeling concept and did not propose a method to implement the concept in the general case. Later, Sun and Grotstollen [24] proposed a similar averaged modeling concept based on the so-called slowly varying amplitude and phase transformation technique. The result is accurate but only the numerical solution can be used to plot the transfer function. The fourth method is the extended describing function method proposed by Yang *et al.* [25]. The describing function technique is extended to a more generalized multivariable case, where state variables are represented by some limited number of harmonic terms. The modulation frequency is limited to one-half of the output ripple frequency from the harmonic balance point of view. Compared with experimental results, this method can predict beat frequency dynamics very accurately.

Although small-signal models shown in [18]–[25] are accurate enough to capture beat frequency dynamics, none of the models is widely used as all of them have complicated mathematics instead of using a circuit-oriented way. Therefore, little physical insight can be extracted from these models. Efforts have also been made to modify or extend these methods to gain some physical insights and are summarized as follows: in [26], an approximated model based on intuition was proposed by Vorperion and it provides good physical insight for low-frequency pole and is able to capture the beat frequency dynamics. This approach is a good combination of simplicity and accuracy, but nonetheless is an approximation and relies on an intuitive rather than a formal derivation. Moreover, the model is not accurate when the switching frequency is close to the resonant frequency. In [27] and [28], a low-frequency continuous time two-port y parameter equivalent circuit model is proposed by Witulski *et al.* based on the discrete-time result. However, this equivalent circuit model is only accurate when perturbation is at low frequency and it cannot predict beat frequency dynamics. In [29], a new modeling technique based on phasor transformation is proposed by Rim and Chao. This approach gives explicit and simple equations with fruitful physical insight. The model captures low-frequency dynamics of the SRC: in the case where the switching frequency deviates from the resonant frequency, the SRC is modeled as the first order, and in the case of resonance, the SRC is modeled as the second order. However, the high-frequency beat frequency dynamics cannot be seen easily in time-domain simulation and the information is lost in the equivalent circuit model. Therefore, it is not accurate enough for the high-bandwidth design. In [30], the equivalent circuit model for the SRC is proposed by Yang *et al.* based on the small-signal modeling results obtained from the extended describing function concept. The equivalent circuit model can well capture the beat frequency dynamics and is as accurate as the describing function result. The major shortcoming of the equivalent circuit model shown in [30] is higher than the usual order of the model; the equivalent circuit model is a fifth-order circuit as there are five energy storage elements. However, the small-signal behavior is found sufficient to be described as a third-order circuit, which is also proved in [24], where the numerical solution shows that the third-order transfer function using the higher order averaging method is almost as accurate as the results obtained from the extended describing function method. Therefore, the equivalent circuit model is still too complicated to extract fruitful physical insight. Furthermore, the transfer functions are still derived based on the numerical solution and no explicit analytical solutions are provided for design purpose.

This paper tries to take the advantage of the accurate results of the equivalent circuit model shown in [30] and overcome the shortcomings related with it. The following two major objectives will be achieved. 1) Simplify the small-signal equivalent circuit model of the SRC to a third-order circuit which is simpler but accurate enough to predict beat frequency dynamics. 2) Provide analytical expressions for all transfer functions to help engineers to design the feedback loop. This paper is an extension of the conference paper [31]. The remaining paper is organized as follows: a brief review of Yang's modeling approach is presented in Section II. In Section III, a third-order small-signal equivalent circuit model is proposed. Section IV discusses two important aspects about the small-signal behavior with the proposed equivalent circuit: dc gain and beat frequency dynamics. Besides, analytical expressions of all transfer functions are presented for easy reference. Section V provides Simplis simulation and experimental results to verify the proposed equivalent circuit model. Section VI summarizes this paper.

II. Brief Review of Yang *et al.* Equivalent Circuit Model [30]

As shown in Fig. 1, for SRC, the tank current does not have dc components but contains strong switching frequency harmonics. Therefore, the averaging concept breaks down. Up to now, the equivalent circuit model proposed by Yang *et al.* in [30] based on the results by the extended describing function concept is the most successful model. During the derivation, fundamental approximation is used, i.e., only fundamental components of the resonant tank variable are considered. Although the total harmonic distortion can be very large when the switching frequency is far away from the resonant frequency, as given in

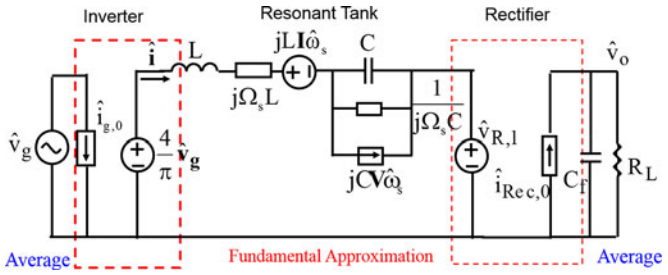

Fig. 2. Small-signal model of SRC.

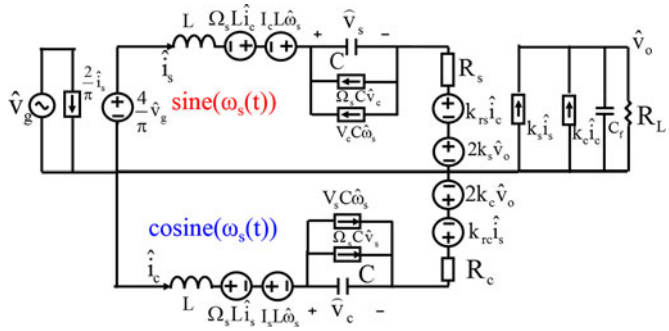

Fig. 3. Small-signal model of SRC suitable for simulation.

[32], even in this condition, the small-signal model using the fundamental component is adequate and accurate for the SRC.

The describing function methods are applied to the inverter, rectifier, and resonant tank, respectively. The small-signal model of the SRC is shown in Fig. 2. For the inverter, the input of the inverter uses average approximation, while the output uses fundamental approximation. For the input side, it is a controlled current source as the average value of the input current is related with the resonant current; for the output side, it is a controlled voltage source as the magnitude of the fundamental component is related with the input voltage.

For the rectifier, the scenario is similar. The input uses fundamental approximation, while the output uses average approximation. For the input side, it is a controlled voltage source as the magnitude of the fundamental component $v_{R,1}$ is related with the output voltage v_o; for the output side, it is a controlled current source as the average value of the output current is related with the resonant current.

For the resonant inductor and resonant capacitor, the fundamental approximation is employed to derive the small-signal model. Although the inductor and capacitor are linear components, the small-signal models are complex as the resonant variables, i.e., resonant current and voltage, have two frequency components: f_m and f_s. In this paper, f (in hertz) is the frequency, while Ω is the angular frequency (in radians/s). Angular frequency Ω is larger than frequency f by a factor of 2π. For the small-signal model, we are interested in the behavior of the modulation frequency. However, the behavior of the modulation frequency is affected by f_s component as it is carried on top of it in order to go through the resonant tank. As seen from Fig. 2, for the resonant inductor, besides the traditional inductor, there is one complex impedance due to the effect of the switching frequency. In addition, there is one complex voltage source due to perturbation of the switching frequency. Similar result can be obtained for the model of the resonant capacitor. As shown in Fig. 2, there are two components in parallel with the traditional capacitor: one is the complex impedance, which is related with the switching frequency; the other is a complex current source, which is controlled by perturbation of the switching frequency.

The issue for the small-signal model shown in Fig. 2 is that this equivalent circuit model cannot be simulated due to the complex term *j* shown in the impedance and controlled sources of the resonant tank model.

To derive an equivalent circuit model suitable for simulation, Yang separates the orthogonal parts into sine part and cosine part, as shown in Fig. 3. By this way, the complex terms disappear but some cross-coupling terms occur. This is reasonable as the complex term in essence changes the sine part into cosine part and vice versa. The equivalent circuit model shown in Fig. 3 is suitable for simulation.

V_s, V_c, I_s, and I_c are derived from steady-state solutions and the results are as follows:

$$\mathbf{I_s} = \frac{4V_g}{\pi}\frac{R_{\rm eq}}{R_{\rm eq}^2+X_{\rm eq}^2}, \mathbf{I_c} = -\frac{4V_g}{\pi}\frac{X_{\rm eq}}{R_{\rm eq}^2+X_{\rm eq}^2}$$

$$\mathbf{V_s} = -\frac{4V_g}{\pi\Omega_s C}\frac{X_{\rm eq}}{R_{\rm eq}^2+X_{\rm eq}^2}, \mathbf{V_c} = -\frac{4V_g}{\pi\Omega_s C}\frac{R_{\rm eq}}{R_{\rm eq}^2+X_{\rm eq}^2}. \quad (1)$$

$X_{\rm eq}$ represents the tank impedance at the switching frequency and $R_{\rm eq}$ represents the equivalent load resistance. The expressions are shown as follows:

$$X_{\rm eq} = \Omega_s L - \frac{1}{\Omega_s C}, R_{\rm eq} = \frac{8}{\pi^2}R_L. \quad (2)$$

Expressions of $k_{\rm rs}$, $k_{\rm rc}$, R_s, R_c, k_s, and k_c are as follows:

$$k_{rs} = k_{rc} = \frac{R_{\rm eq}^2 X_{\rm eq}}{X_{\rm eq}^2+R_{\rm eq}^2}$$

$$k_s = \frac{2}{\pi}\frac{R_{\rm eq}}{\sqrt{R_{\rm eq}^2+X_{\rm eq}^2}}, k_c = -\frac{2}{\pi}\frac{X_{\rm eq}}{\sqrt{R_{\rm eq}^2+X_{\rm eq}^2}}$$

$$R_s = R_{\rm eq}\frac{X_{\rm eq}^2}{X_{\rm eq}^2+R_{\rm eq}^2}, R_c = R_{\rm eq}\frac{R_{\rm eq}^2}{X_{\rm eq}^2+R_{\rm eq}^2}. \quad (3)$$

As shown in [30] and [32], the small-signal equivalent circuit model can well capture the beat frequency dynamics and is very accurate compared with experimental results. However, the order of the equivalent circuit model in Fig. 3 is five and too high as the small-signal behavior is sufficient to be described as a third-order model. More importantly, the transfer functions are still derived based on the numerical solution instead of analytical solutions. This intrigues the continuing work to simplify the equivalent circuit model and derive the analytical solution.

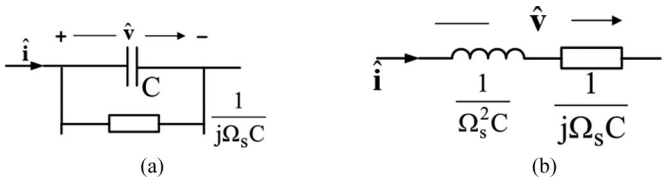

Fig. 4. (a) Original small-signal model of the resonant capacitor at $\hat{\omega}_s = 0$. (b) Equivalent model under $\omega_m \ll \Omega_s$.

III. Proposed Simple Equivalent Circuit Model for the SRC

A. Simplification of the Resonant Capacitor Branch

To simplify the equivalent circuit model, the focus is on the model of the resonant tank. As shown in Fig. 2, the small-signal model of the resonant capacitor is a traditional capacitor with one complex impedance and one controlled current source. It is critical to understand and analyze the effect of the complex impedance and the controlled current course. For simplicity, first, we consider a particular case with no perturbation of the switching frequency. In this case, the controlled current sources disappear, as shown in Fig. 4(a).

To analyze the effect of complex impedance, we do the following mathematical analysis:

$$\frac{\hat{\mathbf{v}}}{\hat{\mathbf{i}}} = \frac{1}{sC + j\Omega_s C} = \frac{1}{j\Omega_s C\left(\frac{s}{j\Omega_s}+1\right)}$$
$$= \frac{-\frac{s}{j\Omega_s}+1}{j\Omega_s C\left(\frac{s}{j\Omega_s}+1\right)\left(-\frac{s}{j\Omega_s}+1\right)} = \frac{-\frac{s}{j\Omega_s}+1}{j\Omega_s C\left(1+\frac{s^2}{\Omega_s^2}\right)}. \tag{4}$$

Under the condition that $\omega_m \ll \Omega_s$, the second term in the denominator is much less than 1 and therefore can be neglected. The simplification leads to the following:

$$\frac{\hat{\mathbf{v}}}{\hat{\mathbf{i}}} \approx \frac{-\frac{s}{j\Omega_s}+1}{j\Omega_s C} = \frac{s}{\Omega_s^2 C} + \frac{1}{j\Omega_s C}. \tag{5}$$

The above equation can be represented using an equivalent circuit, as shown in Fig. 4(b). Very surprisingly, the capacitor in parallel with the complex impedance can be simplified as an equivalent inductor in series with the same complex impedance, with the inductance value determined by the switching frequency and the capacitance value.

This phenomenon is very interesting as it is somewhat against the common sense in the PWM converter: a capacitor and an inductor are two basic energy storage elements with very different dynamic behavior. In other words, there is no such case in the PWM converter that a capacitor can be turned into an inductor. However, the transformation in Fig. 4 shows that in the resonant converter, for low-frequency modulation $\omega_m \ll \Omega_s$, the capacitor behaves like an equivalent inductor with respect to the modulation frequency ω_m. It should be noted that this conclusion is only valid in the case that the modulation signal is carried by the carrier frequency (switching frequency). Therefore, this phenomenon only exists in resonant converters and can never be observed in PWM-type converters.

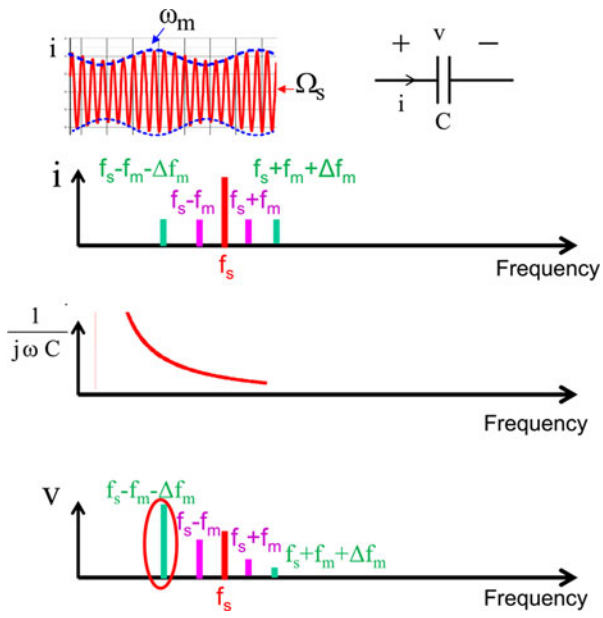

Fig. 5. Frequency spectrum interpretation of the resonant capacitor branch.

The above phenomenon can also be interpreted from spectrum perspective with more physical insights. As shown in Fig. 5, the current in the resonant tank has both the modulation frequency (the envelope) and the switching frequency. The spectrum of the resonant current includes f_s, $f_s - f_m$, and $f_s + f_m$ components. The modulation signal is carried by the sideband components $f_s - f_m$ and $f_s + f_m$. The impedance of the capacitor in the frequency domain is decreasing monotonically. As a result, the voltage on $f_s - f_m$ is dominating. When f_m increases by Δf_m, $f_s - f_m$ moves to lower frequency (see the green bar in the frequency spectrum), the voltage on $f_s - f_m$ also increases. In other words, with respect to the modulation frequency, the voltage increases as the modulation frequency increases. From this perspective, the resonant capacitor behaves like an equivalent inductor: for a traditional inductor, when the modulation frequency of the current increases, the voltage across the inductor also increases as the impedance of the inductor is increasing. As stated previously, this scenario only happens when the modulation frequency signal is carried by the sideband component, which is a special phenomenon in the resonant tank due to the resonant behavior.

Although the above analysis is based on a simple case when $\hat{\omega}_s = 0$, similar conclusion can be drawn for general case. By Thevenin's theorem, the final simplified equivalent circuit model for the resonant capacitor branch can be derived as shown in Fig. 6. The capacitor behaves like an equivalent inductor with respect to the modulation frequency.

With the result shown in Fig. 6, the equivalent circuit model of the resonant tank can be simplified by combining the inductances and complex impedances, as shown in Fig. 7.

One important conclusion is that with respect to the modulation frequency, the resonant tank always shows the inductive behavior. The equivalent inductor of the resonant tank L_e is

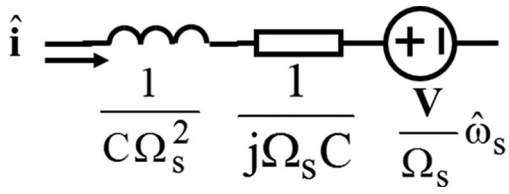

Fig. 6. Simplified equivalent circuit model for the resonant capacitor branch using Thevenin's Theorem.

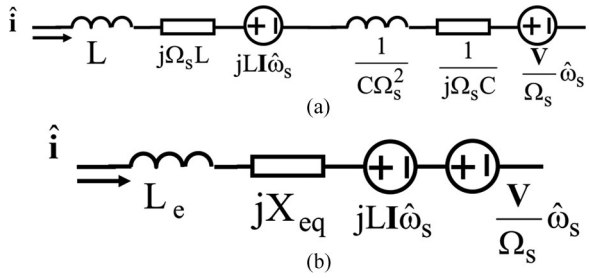

Fig. 7. Simplified equivalent circuit model of the resonant tank: (a) using the result in Fig. 6 and (b) combining the inductances and complex impedances.

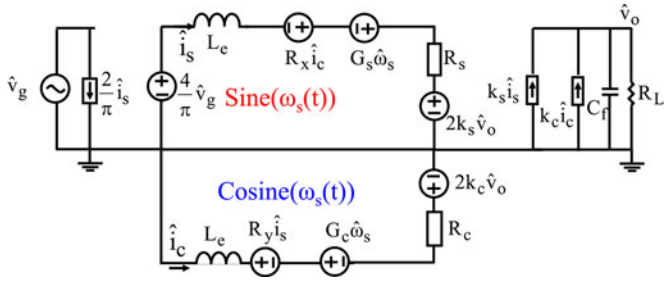

Fig. 8. Simplified third-order equivalent circuit model of SRC.

determined by both L and C, as

$$L_e = L + \frac{1}{C\Omega_s^2} = L\left(1 + \frac{\Omega_o^2}{\Omega_s^2}\right). \tag{6}$$

With a simplified resonant tank, the original small-signal model shown in Fig. 3 can be simplified, as shown in Fig. 8. Compared with the original fifth-order equivalent circuit model shown in Fig. 3, the inverter model and the rectifier model are same, while the tank model is simplified to reduce the circuit order. The dynamic capacitors are transformed into equivalent inductor and therefore disappear, which reduce the order of the model from fifth to third.The expressions of R_s, R_c, k_s, and k_c are shown in (3) and the expressions of L_e, R_x, G_s, R_y, and G_c are shown as follows:

$$\begin{aligned} L_e &= L + \frac{1}{C\Omega_s^2}, R_x = \frac{X_{\rm eq}^3}{X_{\rm eq}^2 + R_{\rm eq}^2}, \\ R_y &= X_{\rm eq} \cdot \frac{X_{\rm eq}^2 + 2R_{\rm eq}^2}{X_{\rm eq}^2 + R_{\rm eq}^2} \\ G_s &= LI_c + \frac{V_s}{\Omega_s}, G_c = LI_s - \frac{V_c}{\Omega_s} \end{aligned} \tag{7}$$

where $X_{\rm eq}$ represents the tank impedance at the switching frequency and $\rm R_{eq}$ represents the equivalent load resistance.

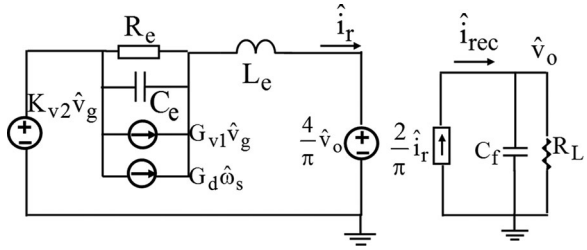

Fig. 9. Proposed noncoupled equivalent circuit model for SRC.

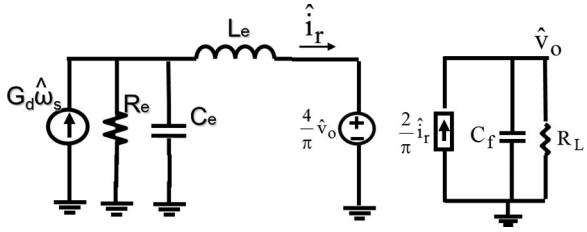

Fig. 10. Noncoupled equivalent circuit model for control-to-output voltage transfer function.

The expressions of $X_{\rm eq}$ and $R_{\rm eq}$ are shown in (2). I_c, V_s, I_s, and V_c are steady-state parameters and shown in (1).

B. Proposed Noncoupled Equivalent Circuit Model

Although the equivalent circuit model shown in Fig. 8 is third order, there is still cross-coupling between the sine branch and cosine branch. The superposition theorem is applied to derive a simple noncoupled equivalent circuit model. The detailed derivation process is shown in the Appendix and the noncoupled equivalent circuit model is shown in Fig. 9:

The expressions of L_e, R_e, C_e, G_{v1}, K_{v2}, and G_d are listed as follows:

$$\begin{aligned} L_e &= L\left(1 + \frac{\Omega_o^2}{\Omega_s^2}\right), C_e = \frac{1}{L_e\left(\Omega_s - \Omega_o\right)^2}, \\ R_e &= \frac{L_e\left|X_{\rm eq}\right|\left|\Omega_s - \Omega_o\right|}{R_{\rm eq}} \\ G_d &= -\frac{4}{\pi}\frac{V_g}{\Omega_s\sqrt{R_{\rm eq}^2 + X_{\rm eq}^2}}\frac{\Omega_s^2 + \Omega_o^2}{\Omega_s^2 - \Omega_o^2}, \\ G_{v1} &= \frac{2}{\pi}\frac{X_{\rm eq}}{\sqrt{X_{\rm eq}^2 + R_{\rm eq}^2}}, K_{v2} = \frac{4}{\pi}\frac{R_{\rm eq}}{\sqrt{X_{\rm eq}^2 + R_{\rm eq}^2}}. \end{aligned} \tag{8}$$

IV. Discussion and Prediction of the Proposed Equivalent Circuit Model

A. DC Gain and Beat Frequency Dynamics of Control to Output Voltage Transfer Function

For the control-to-output voltage transfer function, the terms related with input voltage perturbation are zero and Fig. 9 can be further simplified as shown in Fig. 10.

The three-dimensional (3-D) plot of control to output voltage transfer function can be plotted as shown in Fig. 11.

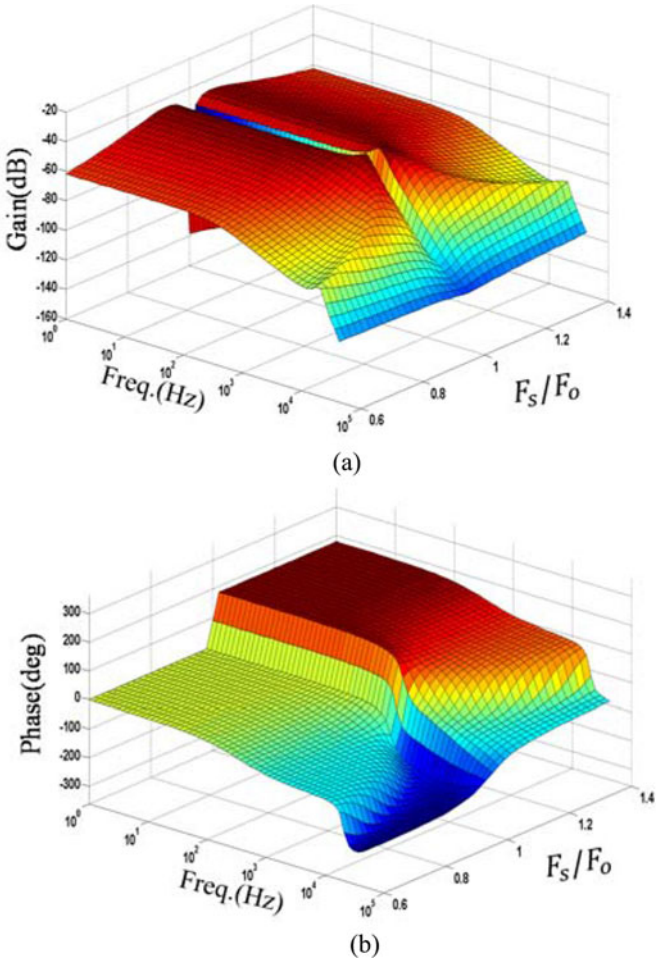

Fig. 11. Three-dimensional Bode plot of control-to-output voltage transfer function. (a) Gain plot. (b) Phase plot.

The dc gain of the control-to-output voltage transfer function can be derived easily as follows:

$$G_{DC} = G_d \cdot R_e \| R_{\rm eq} = \frac{V_g X_{\rm eq} R_{\rm eq} \left(X_{\rm eq}\Omega_s + 2L\Omega_s^2\right)}{\Omega_s^2 \sqrt{X_{\rm eq}^2 + R_{\rm eq}^2}\left(X_{\rm eq}^2 + R_{\rm eq}^2\right)}. \quad (9)$$

The dc gain can be related with the slope of the voltage conversion ratio curve by the following relation:

$$G_{\rm dc} = \frac{\partial V_o}{\partial \Omega_s} = \frac{V_g}{\Omega_o}\frac{\partial M}{\partial \Omega_s}. \quad (10)$$

When $\Omega_s = \Omega_o$, the slope is zero as the curve is at maximum point, therefore, the dc gain is zero which explains the canyon region in the 3-D graph in Fig. 11. When $\Omega_s < \Omega_o$, the slope is positive. When $\Omega_s > \Omega_o$, the slope is negative. This explains the phenomenon observed in 3-D plots in Fig. 11, where 180° phase difference is shown for $\Omega_s < \Omega_o$ and $\Omega_s > \Omega_o$ cases.

The beat frequency dynamic performance of the circuit can also be well explained by the equivalent circuit. The components R_e, C_e, and L_e represent beat frequency dynamics. The equivalent inductor L_e is probably resonant with the equivalent output capacitor or the equivalent capacitor C_e, depending on the value of R_e.

When the switching frequency F_s is far away from the resonant frequency F_o, R_e is large. L_e is resonant with C_e, which forms the beat frequency double pole. The output capacitor and the load resistor form a single pole on the load side. In this case, the double-pole position and its quality factor can be easily derived from Fig. 10 as follows:

$$\omega_{\rm beat} = |\Omega_s - \Omega_o|, Q_{\rm beat} = \frac{\left|\Omega_s L - \frac{1}{\Omega_s C}\right|}{R_{\rm eq}}. \quad (11)$$

When the switching frequency F_s is very close to the resonant frequency F_o, R_e is small. The double pole caused by L_e and C_e will be damped out and split, one moves to high frequency and the other one moves to low frequency. This low-frequency pole will combine with the low-pass filter pole and form a double pole. In other words, L_e resonates with the equivalent output capacitor C_f and the load resistance determines the damping factor of this double pole.

When $\Omega_s = \Omega_o$, the double-pole position and its quality factor are shown as follows: the output impedance can be obtained as follows:

$$\omega_1 = \frac{2}{\pi}\frac{1}{\sqrt{LC_f}}, \quad Q_1 = \frac{2}{\pi}\frac{R_L}{\sqrt{\frac{L}{C_f}}}. \quad (12)$$

The double pole is determined by resonance between tank impedance 2L and the equivalent output capacitor, while the output load determines the quality factor. The tank impedance in this case is 2L with respect to the modulation frequency. One L is from the resonant inductor, the other L is from the resonant capacitor: as shown in Fig. 7(a), the equivalent inductance value of the resonant capacitor is also L. As a result, the total inductance of the resonant tank is 2L.

When $\Omega_s = \Omega_o$, the double-pole position is misunderstood in the literature [32], where it mistakenly states that the double pole is located at the output filter corner frequency.

To explain the beat frequency dynamics more clearly, the two-dimensional Bode plots of Fig. 11 are shown in Fig. 12 as an illustration example: when $\Omega_s = 0.6\,\Omega_o$, $R_e = 360\,\Omega$ is very large, L_e resonates with C_e, $F_{\rm beat} = 20$ kHz, and $Q_{\rm beat} = 5.5$. Shown as the red curve in Fig. 12(a), there is a beat frequency double pole at 20 kHz and a single pole at low frequency caused by the output filter. When $\Omega_s = 0.8\,\Omega_o$, $R_e = 64\,\Omega$ is still very large, L_e resonates with C_e, $F_{\rm beat} = 10$ kHz, and $Q_{\rm beat} = 2.3$. Shown as the blue curve, the beat frequency moves to 10 kHz, while the peaking reduces. When $\Omega_s = 0.95\,\Omega_o$, $R_e = 3\,\Omega$ is smaller, $F_{\rm beat} = 2.5$ kHz, and $Q_{\rm beat} = 0.5$. The beat frequency double pole is about to split. This means that L_e is not only resonates with C_e, but also with the output capacitor C_f. Shown as the black curve, the beat frequency double pole is about to split and no peaking is observed. When $\Omega_s = 0.99\Omega_o$, $R_e = 0.1\,\Omega$ is very small. The beat frequency double pole is split. L_e resonates with the output capacitor C_f. Shown as the pink curve, the double pole formed by L_e and equivalent output capacitor, instead of the beat frequency double pole, is observed. The similar scenario is observed for region $\Omega_s \geq \Omega_o$ shown

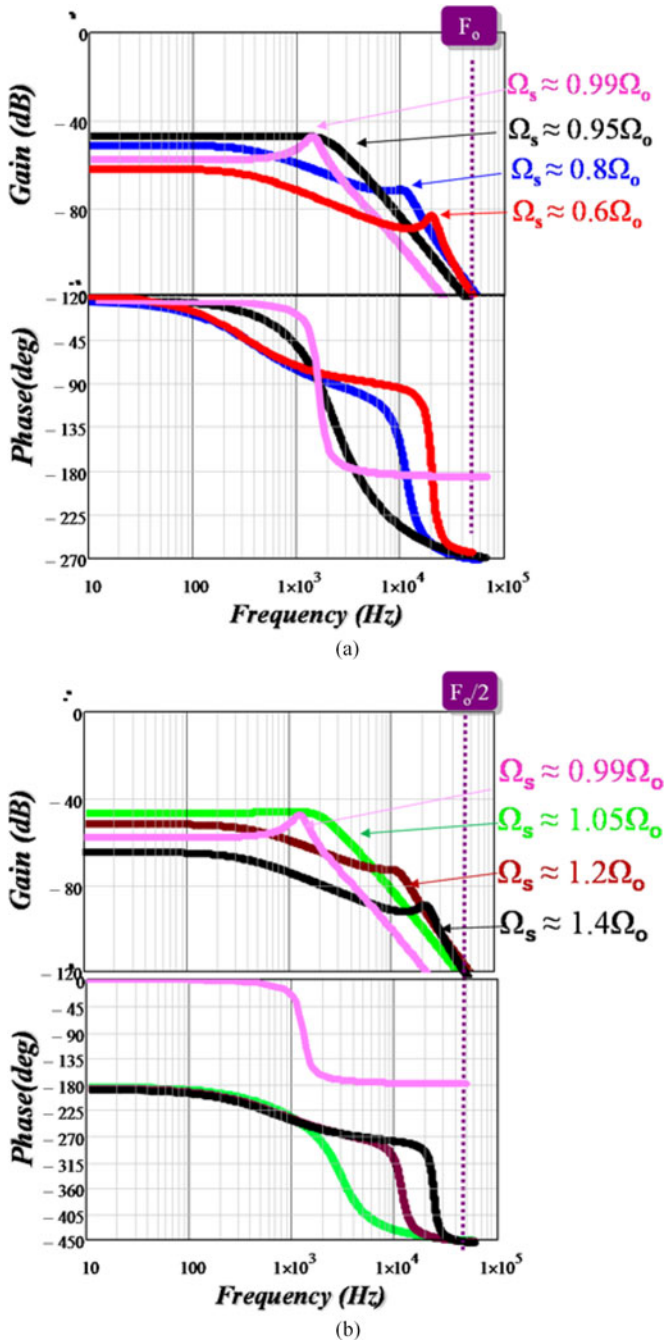

Fig. 12. Illustration example of beat frequency dynamics. (a) For region $\Omega_s \leq \Omega_o$. (b). For region $\Omega_s \geq \Omega_o$.

in Fig. 12(b). For the green curve, $\Omega_s = 1.05\,\Omega_o$, $R_e = 3\,\Omega$, $F_{\text{beat}} = 2.5$ kHz, and $Q_{\text{beat}} = 0.5$. L_e resonates with both C_e and C_f. For the red curve, $\Omega_s = 1.2\,\Omega_o$, $R_e = 43\,\Omega$, $F_{\text{beat}} = 10$ kHz, and $Q_{\text{beat}} = 1.8$. The beat frequency double pole is shown again. L_e resonates only with C_e. For the black curve, $\Omega_s = 1.4\,\Omega_o$, $R_e = 149\,\Omega$, $F_{\text{beat}} = 20$ kHz, and $Q_{\text{beat}} = 3.5$. As the switching frequency is farther away, the beat frequency double pole is more obvious.

In sum, the proposed equivalent circuit model can successfully explain the beat frequency dynamics: when the switching frequency is far away from the resonant frequency, the beat frequency double pole is obvious, and the circuit is third order; when the switching frequency is close to the resonant frequency, the beat frequency will split and the circuit will become second order.

TABLE I
ANALYTICAL EXPRESSIONS OF TRANSFER FUNCTIONS

$$\frac{\hat{v}_o(s)}{\hat{\omega}_s(s)} = \frac{K_d}{(s^2L_e^2 + sL_eR_{\text{eq}} + X_{\text{eq}}^2)(1 + R_LC_fs) + R_{\text{eq}}(sL_e + R_{\text{eq}})}$$
$$K_d = -\frac{V_g}{\Omega_s}\frac{R_{\text{eq}}}{\sqrt{R_{\text{eq}}^2 + X_{\text{eq}}^2}}\frac{\Omega_s^2 + \Omega_o^2}{\Omega_s^2 - \Omega_o^2}X_{\text{eq}}^2 \quad (13)$$

$$\frac{\hat{v}_o(s)}{\hat{v}_g(s)} = \frac{K_v(R_{\text{eq}}^2 + X_{\text{eq}}^2 + L_eR_{\text{eq}}s)}{(s^2L_e^2 + sL_eR_{\text{eq}} + X_{\text{eq}}^2)(1 + R_LC_fs) + R_{\text{eq}}(sL_e + R_{\text{eq}})}$$
$$K_v = \frac{R_{\text{eq}}}{\sqrt{R_{\text{eq}}^2 + X_{\text{eq}}^2}} \quad (14)$$

$$Z_o(s) = \frac{R_L(s^2L_e^2 + sL_eR_{\text{eq}} + X_{\text{eq}}^2)}{(s^2L_e^2 + sL_eR_{\text{eq}} + X_{\text{eq}}^2)(1 + R_LC_fs) + R_{\text{eq}}(sL_e + R_{\text{eq}})} \quad (15)$$

$$Z_{\text{in}}(s) = \frac{\pi^2}{8}\frac{(s^2L_e^2 + sL_eR_{\text{eq}} + X_{\text{eq}}^2)(1 + R_LC_fs) + R_{\text{eq}}(sL_e + R_{\text{eq}})}{s^2L_eC_fR_L + sL_e + sC_fR_L\frac{R_{\text{eq}}^3}{R_{\text{eq}}^2 + X_{\text{eq}}^2} + R_{\text{eq}}} \quad (16)$$

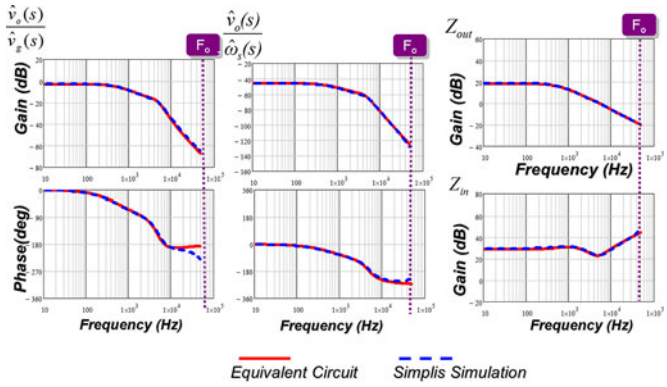

Fig. 13. Simplis verification of the small-signal equivalent circuit model for $Fs = 0.9\,Fo$.

B. Analytical Expressions of Transfer Functions

All the analytical transfer functions can be derived from Figs. 8 and 9, and they are provided in Table I for easy reference. These transfer functions are very helpful in designing the outer feedback compensator. The transfer functions are generally of third order and can be reduced to second order when the switching frequency is very close to the resonant frequency.

V. SIMULATION AND EXPERIMENTAL VERIFICATION

The SIMPLIS simulation tool is used to verify the small-signal analysis. Circuit parameters are as follows: $V_g = 400$ V, $L = 197\ \mu$H, $C = 51$ nF, $F_o = 50.2$ kHz, $C_f = 32\ \mu$F, $R_L = 15.5\,\Omega$, and the corresponding $Q_s = 4$. The comparison results of the equivalent circuit model and simulation results for $F_s = 0.9\,F_o$, $F_s = 1.01F_o$, and $F_s = 1.2\,F_o$ are shown in Figs. 13–15, respectively. In all the graphs, the "equivalent circuit" means the model derived from third-order equivalent circuit models shown in Figs. 8 and 9, while "Simplis Simulation" means the transfer functions from simulation of the real switching circuit. All the transfer functions match very well.

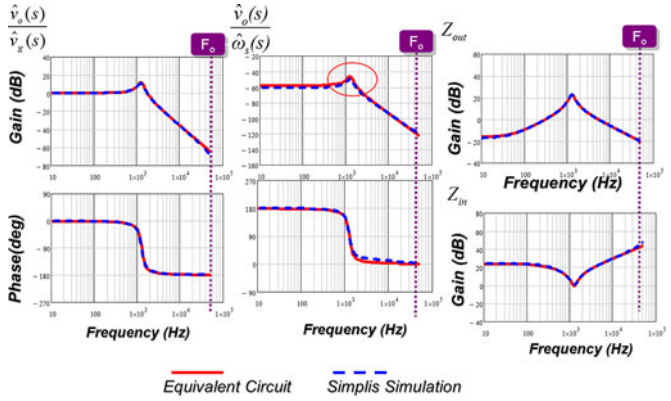

Fig. 14. Simplis verification of the small-signal equivalent circuit model for $Fs = 1.01\,Fo$.

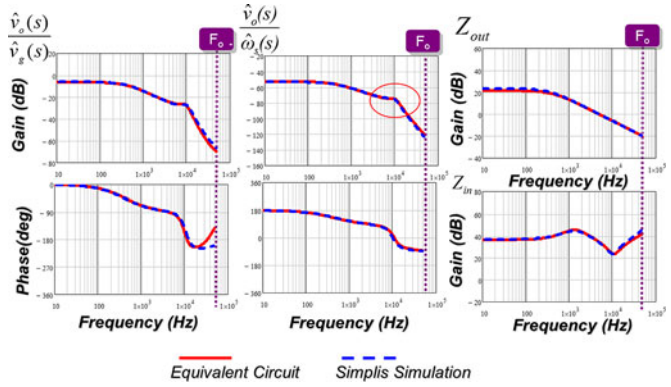

Fig. 15. Simplis verification of the small-signal equivalent circuit model for $Fs = 1.2\,Fo$.

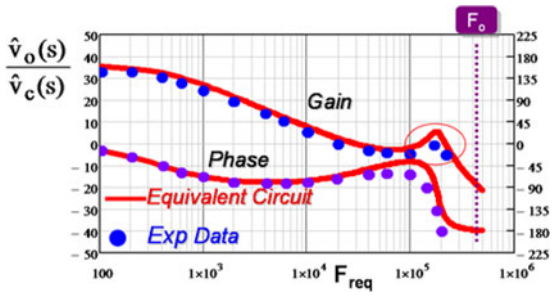

Fig. 16. Experimental verification of the control-to-output transfer function for $Fs = 0.56Fo$ and $Qs = 2.2$. The experimental data are taken from [32].

The experimental verifications are shown in Figs 16 and 17. The experimental data for Fig. 16 are taken from [32] and the circuit parameters are $L = 22.5\ \mu$H, $C = 6.56$ nF, $F_o = 414$ kHz, and $C_f = 16.75\ \mu$F. The gain in the voltage-controlled oscillator is 450 k. Compared with experimental data, the control-to-output voltage predictions from equivalent circuits shown in Figs 8 and 9 are very good and the beat frequency double pole is accurately predicted. The experimental data for Fig. 17 are taken from [33] and the circuit parameters are $L = 197\ \mu$H, $C = 51$ nF, $F_o = 50.2$kHz, and $C_f = 32\ \mu$F. The input impedance from the equivalent circuit shown in Fig. 8 is also very accurate compared with measurement.

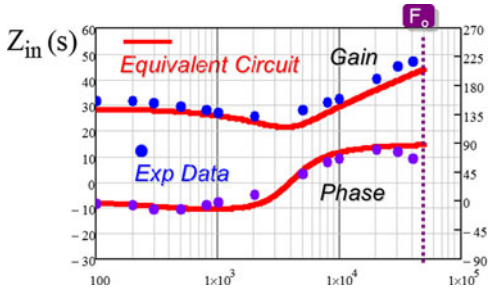

Fig. 17. Experimental verification of the input impedance transfer function for $Fs = 0.92\,Fo$ and $Qs = 4$. The experimental data are taken from [33].

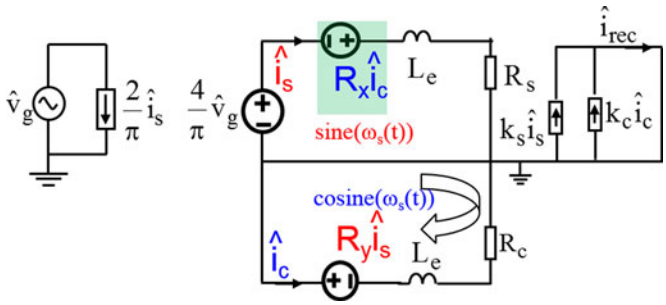

Fig. 18. Equivalent circuit model for derivation of G_{vg}.

VI. Summary and Conclusion

This paper proposes a third-order equivalent circuit for the SRC. The equivalent circuit model is based on the fact that with respect to the modulation frequency, the behavior of the resonant capacitor is equivalent to an inductor. The proposed third-order equivalent circuit model can be used to explain all the phenomena such as the beat frequency dynamics. For the first time, analytical solutions are provided for all the transfer functions and this will be a very helpful tool for the feedback design.

Appendix

A. Derivation of the NonCoupled Equivalent Circuit Model (see Fig. 9)

In the Appendix, the superposition theorem is applied to derive a noncoupled equivalent circuit model, starting from the simplified third-order equivalent circuit model, as shown in Fig. 8.

The output current is affected by the input voltage perturbation, output voltage perturbation, and switching frequency perturbation, as shown in Fig. 8:

G_{vg}, G_{vs}, and G_{vo} are first derived separately using circuit techniques, then, the total response of the output current is obtained by adding the individual response as shown in (A1).

Step 1: Derivation of G_{vg}.

The perturbation of v_o and ω_s are set to be zero for derivation of G_{vg}. Then, Fig. 8 can be simplified to Fig. 18.

To decouple Fig. 18, the focus is on the coupled term. Using Kirchhoff's voltage law of the cosine part circuit, the relation of the sine part current and cosine part current can be derived, as

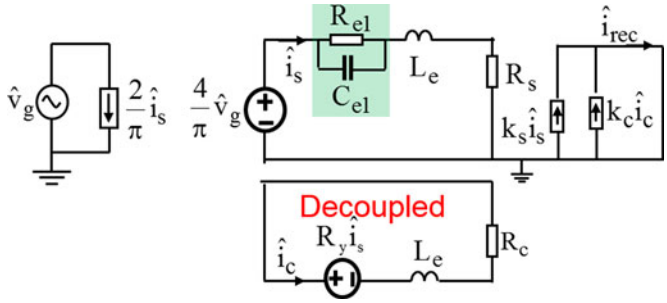

Fig. 19. Equivalent circuit model using the equivalent *RC* branch for derivation of G_{vg}.

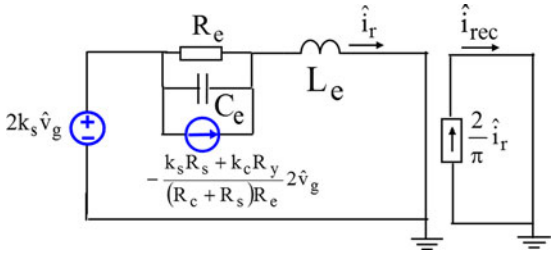

Fig. 20. Noncoupled equivalent circuit model for G_{vg}.

shown in (A2)

$$\hat{i}_{\rm rec}(s) = G_{vg}(s)\hat{v}_g(s) + G_{vs}\hat{\omega}_s(s) + G_{vo}(s)\hat{v}_o(s)S$$

$$G_{vg} = \left.\frac{\hat{i}_{\rm rec}(s)}{\hat{v}_g(s)}\right|_{\hat{v}_o=0,\hat{\omega}_s=0},$$

$$G_{vs} = \left.\frac{\hat{i}_{\rm rec}(s)}{\hat{\omega}_s(s)}\right|_{\hat{v}_g=0,\hat{v}_o=0},$$

$$G_{vo} = \left.\frac{\hat{i}_{\rm rec}(s)}{\hat{v}_o(s)}\right|_{\hat{v}_g=0,\hat{\omega}_s=0} \quad \text{(A1)}$$

$$\hat{i}_c = -\frac{R_y\hat{i}_s}{sL_e + R_c}. \quad \text{(A2)}$$

Then, the coupled voltage source controlled by the cosine part current which is in light blue shade in Fig. 18 can be expressed as

$$-R_x\hat{i}_c = \hat{i}_s\,(R_{e1}//C_{e1})$$

$$R_{e1} = \frac{R_xR_y}{R_c}, C_{e1} = \frac{L_e}{R_xR_y}. \quad \text{(A3)}$$

Therefore, this voltage source can be replaced by an impedance comprised of an equivalent resistor and equivalent capacitor, as shown in Fig. 19. The coupling effect is represented by an equivalent *RC* branch. From the output current point of view, the two output current source can be further combined and simplified, as shown in Fig. 20.

The expressions for Re and Ce are as follows:

$$R_e = \frac{R_{e1}+R_s}{1+R_{e1}C_{e1}R_s/L_e} = \frac{R_xR_y+R_sR_c}{R_s+R_c}$$

$$C_e = C_{e1}\frac{R_{e1}}{R_{e1}+R_s} = \frac{L_e}{R_xR_y+R_sR_c}. \quad \text{(A4)}$$

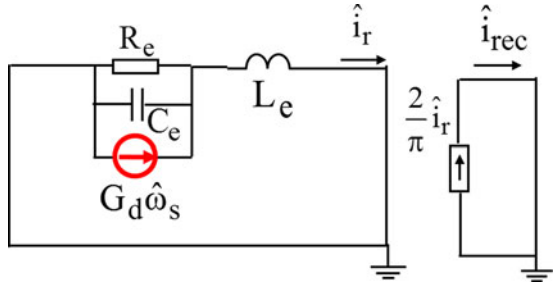

Fig. 21. Noncoupled equivalent circuit model for G_{vs}.

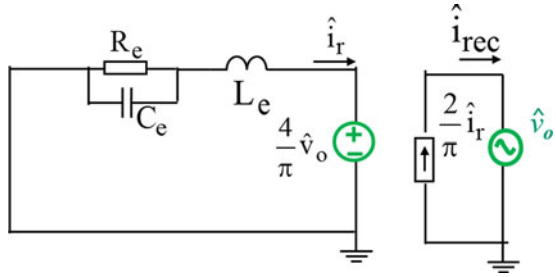

Fig. 22. Noncoupled equivalent circuit model for G_{vo}.

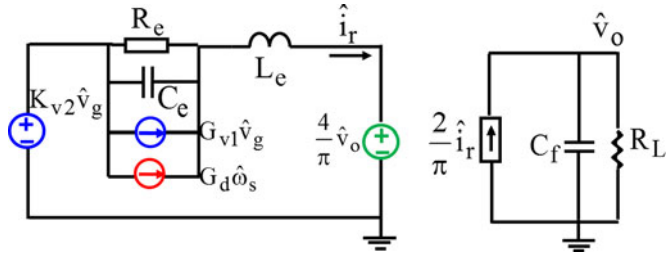

Fig. 23. Final Noncoupled equivalent circuit model for SRC.

Steps 2 and 3: Derivation of G_{vs} and G_{vo}.

The derivation methodology is similar and the results are shown in Figs. 21 and 22, respectively.

The final equivalent circuit model can be derived by combination of Figs. 20, 21, and 22 using the superposition theory. The final equivalent circuit is shown in Fig. 23, which is same as Fig. 9, and the expressions of the parameters are shown in (8).

REFERENCES

[1] G. W. Wester and R. D. Middlebrook, "Low Frequency characterization of switched dc-to-dc converters," in *Proc. IEEE Power Electronic. Spec. Conf.*, 1972, pp. 9–20.

[2] R.D. Middlebrook and S. Cuk, "A general unified approach to modeling switching-converter power stages" in *Proc. IEEE Power Electronic. Spec. Conf.*, 1976, pp. 18–34.

[3] R. Tymerski, V. Vorperian, F. C. Lee and W. T. Baumann, "Nonlinear modeling of the PWM switch," *IEEE Trans. Power Electron.*, vol. 4, no. 2, pp. 225–233, Apr. 1989.

[4] V. Vorperian, "Simplified analysis of PWM converters using model of PWM switch: Continuous conduction mode," *IEEE Trans. Aerosp.*, vol. 26, no. 3, pp. 490–496, May 1990.

[5] J. Li and F. C. Lee, "New modeling approach and equivalent circuit representation for current mode control," *IEEE Trans. Power Electron.*, vol. 25, no. 5, pp. 1218–1230, May 2010.

[6] Y. Yan, F. C. Lee, and P. Mattavelli, "Unified three-terminal switch model for current mode controls," *IEEE Trans. Power Electron.*, vol. 27, no. 9, pp. 4060–4070, Sep. 2012.

[7] S. Tian, F. C. Lee, J. Li, Q. Li, and P. Liu, "Equivalent circuit model of constant on-time current mode control with external ramp compensation," in *Proc. IEEE Energy Convers. Congr. Expo.*, 2014, pp. 3747–3754.
[8] J. Li and F. C. Lee, "Modeling of V2 current-mode control," *IEEE Trans. Circuits Syst. I, Reg. Papers*, vol. 57, no. 9, pp. 2552–2563, Mar. 2010.
[9] S. Tian, F. C. Lee, P. Mattavelli, K. Cheng and Y. Yan, "Small-signal analysis and optimal design of external ramp for constant on-time V2 control with multilayer ceramic caps," *IEEE Trans. Power Electron.*, vol. 29, no. 8, pp. 4450–4460, Aug. 2014.
[10] S. Tian, F. C. Lee, P. Mattavelli and Y. Yan, "Small-signal analysis and optimal design of constant frequency V2 control," *IEEE Trans. Power Electron.*, vol. 30, no. 3, pp. 1724–1733, Mar. 2015.
[11] S. Tian, F. C. Lee, Q. Li, and Y. Yan, "Unified equivalent circuit model and optimal design of V^2 controlled buck converters," *IEEE Trans. Power Electron.*, vol. PP, no. 99, 2015, IEEE Early Access Articles.
[12] F.C. Schwarz, "An improved method of resonant current pulse modulation for power converters," *IEEE Trans. Ind. Electron. Control Instrum.*, vol. IECI-23, no. 2, pp. 133–141, May 1976.
[13] F.C. Schwarz and J. B. Klaasens, "A 95-percent efficient 1-kW converter with an internal frequency of 50kHz," *IEEE Trans. Ind. Electron. Control Instrum.*, vol. IECI-25, no. 4, pp. 326–333, Nov. 1978.
[14] R. R. Robson and P. J. Hancock, "A 10kW series resonant converter design, transistor characterization and base drive optimization," in *Proc. IEEE Power Electron. Spec. Conf.*, Jun. 1982, pp. 33–44.
[15] R. Robson, "Advances in series resonant inverter technology and its effect on spacecraft employing electric propulsion," presented at the AIAA/JSASS/DGLR 16th Int. Electr. Propul. Conf., New Orleans, LA, USA, Nov. 1982.
[16] R. R. Robson, "25 kW resonant dc/dc power converter," Hughes Res. Lab., Nat. Aeronautics Space Admin., Washington, DC, USA, Rep. NASA CR-168273, Sep. 1983.
[17] J. Yu, "Application of series resonant converter in laser power supply," in *Proc. Int. Conf. Electr. Control Eng.*, 2010, pp. 3377–3380.
[18] V. Vorperian and S. Cuk, "Small-signal analysis of resonant converters," in *Proc. IEEE Power Electron. Spec. Conf.*, 1983, pp. 269–282.
[19] R. King and T. Stuart, "Small-signal model for the series resonant converter," *IEEE Trans. Aerosp. Electron. Syst.*, vol. AES-21, no. 3, pp. 301–319, May 1985.
[20] M. G. Kim and M. J. Youn, "A discrete time domain modeling and analysis of controlled series resonant converter," *IEEE Trans. Ind. Electron.*, vol. 38, no. 1, pp. 32–40, Feb. 1991.
[21] G. C. Verghese, M. E. Elbuluk and J. G. Kassakian, "A general approach to sampled-data modeling for power electronic circuits," *IEEE Trans. Power Electron.*, vol. PE-1, no. 2, pp. 76–89, Apr. 1986.
[22] M. E. Elbuluk, G. C. Verghese and J. G. Kassakian, "Sampled-data modeling and digital control of resonant converters," *IEEE Trans. Power Electron.*, vol. 3, no. 3, pp. 344–354, Jul. 1988.
[23] S. Sanders, J. Noworolski, X. Liu, and G. Verghese, "Generalized averaging method for power conversion circuits," *IEEE Trans. Power Electron.*, vol. 6, no. 2, pp. 251–259, Apr. 1991.
[24] J. Sun and H. Grotstollen, "Averaged modeling and analysis of resonant converters," in *Proc. IEEE Power Electron. Spec. Conf.*, 1993, pp. 707–713.
[25] E. X. Yang, F. C. Lee and M. M. Jovanovic, "Small-signal modeling of power electronic circuits by extended describing function concept," in *Proc. Virginia Power Electron. Center Seminar*, 1991, pp. 167–178.
[26] V. Vorperian, "Approximate small-signal analysis of the series and the parallel resonant converters," *IEEE Trans. Power Electron.*, vol. 4, no. 1, pp. 15–24, Jan. 1989.
[27] A. F. Witulski and R. W. Erickson, "Small-signal AC equivalent circuit modeling of the series resonant converter," in *Proc. IEEE Power Electron. Spec. Conf.*, 1987, pp. 693–704.
[28] A. F. Witulski, A. F. Hernadez, and R. W. Erickson, "Small-signal equivalent circuit modeling of resonant converters," *IEEE Tran. Power Electron.*, vol. 6, no. 1, pp. 11–27, Jan. 1991.
[29] C. T. Rim and G. H. Cho, "Phasor transformation and its application to the DC/AC analysis of frequency phase-controlled series resonant converters," *IEEE Trans. Power Electron.*, vol. 5, no. 2, pp. 201–211, Apr. 1990.
[30] E. X. Yang, F. C. Lee, and M. M. Jovanovic, "Small-signal modeling of series and parallel resonant converters," in *Proc. IEEE Appl. Power Electron. Conf.*, 1992, pp. 785–792.
[31] S. Tian, F. C. Lee, Q. Li, and B. Li, "Small-signal equivalent circuit model of series resonant converter," in *Proc. IEEE Energy Convers. Congr. Expo.*, Sep. 2015, accepted for published.
[32] E. X. Yang, "Extended describing function method for small-signal modeling of resonant and multi-resonant converters," Ph.D. dissertation, Dept. Elect. Comput. Eng., Virginia Tech, Blacksburg, VA, USA, Feb. 1994.
[33] V. Vorperian, "Analysis of Resonant Converters," Ph.D. dissertation, Dept. Elect. Comput. Eng., Cal. TechCalifornia Inst. Technol., Pasadena, CA, USA, May 1984, p. 169.

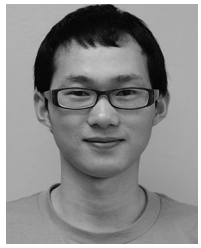

Shuilin Tian (S'11) received the B.S. degree in electrical engineering from Zhejiang University, Hangzhou, China, in 2008, and the M.S. degree in power electronics from the Center for Power Electronics Systems, Virginia Tech, Blacksburg, VA, USA, in April 2012, where he is currently working toward the Ph.D. degree.

From May 2012 to August 2012, he was an Application Engineer Intern in Linear Technology, Milpitas, CA, USA. His research interests include modeling, analysis, and control of pulse width modulation converters (including point of load converters and voltage regulator) and resonant converters.

Fred C. Lee (S'72–M'74–SM'87–F'90–LF'12) received the B.S. degree in electrical engineering from National Cheng Kung University, Tainan City, Taiwan, in 1968, and the M.S. and Ph.D. degrees in electrical engineering from Duke University, Durham, NC, USA, in 1972 and 1974, respectively.

He is currently a University Distinguished Professor at Virginia Polytechnic Institute and State University, Blacksburg, VA, USA, and the Founder and Director of the Center for Power Electronics Systems. He holds 72 U.S. patents, and has published 252 journal articles and 639 refereed technical papers.

Dr. Lee has served as the President of the IEEE Power Electronics Society (1993–1994). He received the William E. Newell Power Electronics Award in 1989, the Arthur E. Fury Award for Leadership and Innovation in 1998, the Honorary Sun Yuen Chuan Chair Professor at National Tsinghua University, Hsinchu, Taiwan, in 2001, the Outstanding Alumni Award from National Cheng Kung University, Tainan, Taiwan, in 2004, the Ernst–Blickle Award for achievement in the field of power electronics in 2005, and the Honorary Kwoh-Ting Li Chair Professor Award at National Cheng Kung University, in 2011. He is a member of the National Academy of Engineering in United States and an academician of Academia in Taiwan.

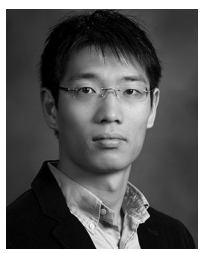

Qiang Li (M'12) received the B.S. and M.S. degrees in power electronics from Zhejiang University, Hangzhou, China, in 2003 and 2006, respectively, and the Ph.D. degree from Virginia Tech, Blacksburg, VA, USA, in 2011.

He is currently an Assistant Professor in the Center for Power Electronics Systems, Virginia Tech. His research interests include distributed power systems, high-frequency power conversion, and high-density electronics packaging and integration.